NeuroImage: Clinical 14 (2017) 286–297

Contents lists available at ScienceDirect

NeuroImage: Clinical

journal homepage: www.elsevier.com/locate/ynicl

Network degeneration and dysfunction in presymptomatic *C9ORF72* expansion carriers

Suzee E. Lee[a,*], Ana C. Sias[a], Maria Luisa Mandelli[a], Jesse A. Brown[a], Alainna B. Brown[a], Anna M. Khazenzon[a,b], Anna A. Vidovszky[a], Theodore P. Zanto[c], Anna M. Karydas[a], Mochtar Pribadi[d], Deepika Dokuru[d], Giovanni Coppola[d], Dan H. Geschwind[d], Rosa Rademakers[e], Maria Luisa Gorno-Tempini[a], Howard J. Rosen[a], Bruce L. Miller[a], William W. Seeley[a,f]

[a] *University of California, San Francisco, Memory and Aging Center, Department of Neurology, 675 Nelson Rising Lane, MC:1207, San Francisco, CA 94158, USA*
[b] *Stanford University, Department of Psychology, Jordan Hall, 450 Serra Mall, Stanford, CA 94305, USA*
[c] *University of California, San Francisco, Department of Neurology, 675 Nelson Rising Lane, MC: 0444, San Francisco, CA 94158, USA*
[d] *Department of Neurology and Department of Psychiatry, Semel Institute for Neuroscience and Human Behavior, University of California, Los Angeles, 760 Westwood Plaza Los Angeles, CA 90024, USA*
[e] *Mayo Clinic, Department of Neuroscience, Birdsall Research Building 207, 4500 San Pablo Road, Jacksonville, FL 32224, USA*
[f] *University of California, San Francisco, Department of Pathology, 675 Nelson Rising Lane, Suite 140, MC:1207, San Francisco, CA 94158, USA*

ARTICLE INFO

Article history:
Received 23 August 2016
Received in revised form 6 December 2016
Accepted 8 December 2016
Available online 10 December 2016

Keywords:
Frontotemporal dementia
Amyotrophic lateral sclerosis
Functional MRI
Diffusion tensor imaging
Genetics

ABSTRACT

Hexanucleotide repeat expansions in *C9ORF72* are the most common known genetic cause of familial and sporadic frontotemporal dementia and amyotrophic lateral sclerosis. Previous work has shown that patients with behavioral variant frontotemporal dementia due to *C9ORF72* show salience and sensorimotor network disruptions comparable to those seen in sporadic behavioral variant frontotemporal dementia, but it remains unknown how early in the lifespan these and other changes in brain structure and function arise. To gain insights into this question, we compared 15 presymptomatic carriers (age 43.7 ± 10.2 years, nine females) to matched healthy controls. We used voxel-based morphometry to assess gray matter, diffusion tensor imaging to interrogate white matter tracts, and task-free functional MRI to probe the salience, sensorimotor, default mode, and medial pulvinar thalamus-seeded networks. We further used a retrospective chart review to ascertain psychiatric histories in carriers and their non-carrier family members. Carriers showed normal cognition and behavior despite gray matter volume and brain connectivity deficits that were apparent as early as the fourth decade of life. Gray matter volume deficits were topographically similar though less severe than those in patients with behavioral variant frontotemporal dementia due to *C9ORF72*, with major foci in cingulate, insula, thalamus, and striatum. Reduced white matter integrity was found in the corpus callosum, cingulum bundles, corticospinal tracts, uncinate fasciculi and inferior longitudinal fasciculi. Intrinsic connectivity deficits were detected in all four networks but most prominent in salience and medial pulvinar thalamus-seeded networks. Carrier and control groups showed comparable relationships between imaging metrics and age, suggesting that deficits emerge during early adulthood. Carriers and non-carrier family members had comparable lifetime histories of psychiatric symptoms. Taken together, the findings suggest that presymptomatic *C9ORF72* expansion carriers exhibit functionally compensated brain volume and connectivity deficits that are similar, though less severe, to those reported during the symptomatic phase. The early adulthood emergence of these deficits suggests that they represent aberrant network patterning during development, an early neurodegeneration prodrome, or both.

Abbreviations: ALS, amyotrophic lateral sclerosis; bvFTD, behavioral variant frontotemporal dementia; FTD, frontotemporal dementia; CDR, Clinical Dementia Rating scale; DMN, default mode network; FA, fractional anisotropy; fMRI, functional MRI; FWE, familywise error; HC, healthy control; ICN, intrinsic connectivity network; IRI, Interpersonal Reactivity Index; MMSE, Mini-Mental State Exam; MND, motor neuron disease; NPI, Neuropsychiatric Inventory; preSxC9, presymptomatic *C9ORF72* expansion carriers; SMN, sensorimotor network; TIV, total intracranial volume; ROI, region of interest; VBM, voxel-based morphometry.

* Corresponding author.
E-mail addresses: Suzee.Lee@ucsf.edu (S.E. Lee), Ana.Sias@ucsf.edu (A.C. Sias), MariaLuisa.Mandelli@ucsf.edu (M.L. Mandelli), Jesse.Brown@ucsf.edu (J.A. Brown), Alainna.brown@gmail.com (A.B. Brown), annakhaz@stanford.edu (A.M. Khazenzon), annavidovszky@yahoo.com (A.A. Vidovszky), Theodore.Zanto@ucsf.edu (T.P. Zanto), Anna.Karydas@ucsf.edu (A.M. Karydas), mochtarpribadi@gmail.com (M. Pribadi), drdokuru@gmail.com (D. Dokuru), gcoppola@ucla.edu (G. Coppola), dhg@mednet.ucla.edu (D.H. Geschwind), Rademakers.Rosa@mayo.edu (R. Rademakers), MariaLuisa.GornoTempini@ucsf.edu (M.L. Gorno-Tempini), Howie.Rosen@ucsf.edu (H.J. Rosen), Bruce.Miller@ucsf.edu (B.L. Miller), Bill.Seeley@ucsf.edu (W.W. Seeley).

http://dx.doi.org/10.1016/j.nicl.2016.12.006

1. Introduction

The preclinical stages of frontotemporal dementia (FTD) remain unclear, in part because the relatively low prevalence of FTD impedes detection of asymptomatic disease in post-mortem brain tissue. Disease-causing mutations afford an important opportunity to study preclinical disease. The *C9ORF72* hexanucleotide (GGGGCC) repeat expansion is the most common known genetic cause of FTD and amyotrophic lateral sclerosis (ALS) and most often presents with behavioral variant FTD (bvFTD), bvFTD with motor neuron disease (bvFTD-MND), or ALS (DeJesus-Hernandez et al., 2011; Renton et al., 2011). While *C9ORF72*-bvFTD and sporadic bvFTD share regional vulnerability in the anterior cingulate and frontoinsular cortices, *C9ORF72*-bvFTD shows additional atrophy in the medial pulvinar nucleus of the thalamus (Lee et al., 2014), parieto-occipital cortex (Beckmann et al., 2005; Irwin et al., 2013; Sha et al., 2012; Whitwell et al., 2012) and, less consistently, cerebellum (Irwin et al., 2013; Mahoney et al., 2012; Whitwell et al., 2012). In ALS, patients with the *C9ORF72* expansion also show greater thalamic involvement (Bede et al., 2013) and more pronounced frontal and anterior cingulate atrophy compared to sporadic ALS (Byrne et al., 2012). These findings from symptomatic *C9ORF72*-bvFTD and -ALS provide the anatomical backdrop for studies of presymptomatic *C9ORF72* expansion carriers (preSxC9), who are at risk for either or both of these syndromes.

Limited information is available about brain structure in preSxC9. One recent region-of-interest based study of gray matter volume in 18 preSxC9 suggested that gray matter reductions may have emerged 25 years prior to predicted symptom onset, especially in the thalamus, hippocampus, insula, and parieto-occipital cortex (Rohrer et al., 2015). Another similar study showed temporo-parieto-occipital cortex and striatal deficits in 16 preSxC9 (Walhout et al., 2015). To date, no voxelwise whole brain analyses have defined the gray matter deficit pattern in preSxC9. Only one study has probed for white matter abnormalities in preSxC9 and found no differences compared to controls (Walhout et al., 2015), and no studies have yet explored functional network abnormalities in preSxC9. Previously, we found intrinsic connectivity network (ICN) dysfunction even in single patients with early-stage *C9ORF72*-bvFTD who lacked structural brain atrophy (Lee et al., 2014). Therefore, we hypothesized that preSxC9 would show most prominent network dysfunction in salience, sensorimotor, and medial pulvinar-seeded networks, mirroring the pattern seen in *C9ORF72*-bvFTD. Considering that some patients with *C9ORF72*-bvFTD show prominent psychiatric symptoms (Boeve et al., 2012; Sha et al., 2012; Simón-Sánchez et al., 2012; Snowden et al., 2012), we further hypothesized that the gray matter volume deficits in preSxC9 would be accompanied by a higher rate of psychiatric symptoms compared to non-carrier family members.

Here, we describe the convergent morphometric and brain connectivity deficits seen in 15 preSxC9 compared to matched healthy controls. Hypothesizing that these deficits represent incipient neurodegeneration, we sought regions whose brain imaging metrics declined more sharply with age in preSxC9 than in controls. Finally, we compared rates of psychiatric symptoms in preSxC9 and their non-carrier family members, reasoning that psychiatric symptoms might represent a prodromal correlate of the observed neuroanatomical deficits.

2. Materials and methods

2.1. Participants

We screened the University of California, San Francisco Memory and Aging Center database for *C9ORF72* expansion carriers. PreSxC9 were defined as *C9ORF72* carriers with a Mini-Mental State Exam (MMSE) score ≥ 27 (Folstein et al., 1983) who (1) were asymptomatic and (2) had no upper or lower motor neuron signs on neurological examination. All 15 preSxC9 had a structural MRI scan and were included in the study. A subset of 12 and 13 preSxC9 also had DTI and task-free fMRI scans, respectively. We calculated estimated time to symptom onset by averaging the age of onset among family members with neurodegenerative disease, following previous methods (Rohrer et al., 2015).

Inclusion criteria for all healthy controls in the study were an MMSE score ≥ 27, no significant history of neurological disease, and a brain MRI free of structural lesions, including significant white matter changes. *C9ORF72*-family members who met these healthy control criteria were also included as controls when imaging data were available and when they matched demographic characteristics of the preSxC9 group. Healthy control group 1 (n = 46, HC1) was matched to the preSxC9 for age, sex, education, and handedness for comparison of neuropsychological measures.

All preSxC9 and HC1 underwent a history and physical examination by a behavioral neurologist and a standardized battery of cognitive tests administered by a neuropsychologist. Neurological and neuropsychological assessments occurred within 180 days of MRI scanning. Clinical diagnoses were rendered at a multidisciplinary consensus conference. Informant interviews were used to complete the Frontotemporal Lobar Degeneration-modified Clinical Dementia Rating (CDR) scale to evaluate functional status (Knopman et al., 2008), the Neuropsychiatric Inventory (NPI) to measure behavioral symptoms (Cummings et al., 1994), and the Interpersonal Reactivity Index (IRI) to measure emotional empathy (Davis, 1983). All preSxC9 had CDR total and sum of boxes scores of 0. A CDR was available for 43/46 HC1 and was zero in all.

All 15 preSxC9 had a high-resolution T1-weighted structural MRI available. For voxel-based morphometry (VBM) analyses, we expanded our HC1 group by adding 21 young healthy controls without neurological or psychiatric disease (for whom neuropsychological data were unavailable) to increase statistical power and to better match the age distribution of the preSxC9 group. This combined healthy control group (HC2) of 67 participants was matched to the preSxC9 group for age, sex, and handedness (Supplementary Table 1). PreSxC9 and HC2 showed similar use of central nervous system-acting medications including antidepressant medications for non-psychiatric indications and sleep aids ($\chi^2 = 0.1$, df = 1, p = 0.74).

PreSxC9 with DTI and task-free fMRI data were compared to a smaller group of 30 matched healthy controls (HC3, Supplementary Tables 2 and 3), because fewer matched controls had available DTI and fMRI. One of the HC3 DTI scans was omitted because of slice-wise intensity disruption artifact, thus there were 29 DTI controls. All HC subjects had a brain MRI free of significant white matter changes or other lesions.

The University of California, San Francisco Committee on Human Research approved the study. Participants provided informed consent prior to participation.

2.2. Genetic analysis

The presence of a pathological expansion, larger than 40–50 repeats but not further quantified, within *C9ORF72* was detected using a repeat-primed polymerase chain reaction, as previously described (DeJesus-Hernandez et al., 2011). All preSxC9 screened negative for *MAPT* and *GRN* mutations.

2.3. Image acquisition

All subjects underwent MRI scanning on a Siemens Tim Trio 3 T scanner. For T1-weighted and task-free fMRI images, acquisition followed previous methods (Lee et al., 2014). For diffusion tensor imaging, a high angular resolution diffusion-weighted imaging dataset was acquired using a single-shot spin-echo echo-planar imaging sequence including 55 contiguous axial slices acquired in an interleaved order with the following parameters: in-plane resolution 2.2 mm^2; slice thickness 2.2 mm; TR/TE 8000/109 ms; flip angle 90°; matrix size 100 × 100; 64 non-collinear diffusion sensitization directions at b = 2000 s/mm 2,

11 at b = 0, and an integrated parallel acquisition technique acceleration factor of 2.

2.4. Experimental design

2.4.1. Image processing and analysis

2.4.1.1. Voxel-based morphometry. Voxel-based morphometry was performed using SPM12 (http://www.fil.ion.ucl.ac.uk/spm/) (see Supplementary Methods: VBM preprocessing for details). We compared smoothed, normalized gray matter maps between preSxC9 and healthy controls by using a two-sample *t*-test via the general linear model framework in SPM12. Nuisance covariates included age, sex, handedness and total intracranial volume (TIV). Analyses were thresholded at $p < 0.001$ uncorrected and $p < 0.05$ familywise error (FWE) corrected. Using MARSBAR (Brett et al., 2002), we extracted the mean gray matter intensity within the preSxC9 < HC2 map (for $p < 0.001$ uncorrected and then for pFWE < 0.05) for each participant and plotted the values versus age for visualization purposes only. We then performed an ANCOVA to test for an interaction between age and gene status on gray matter volume, in order to determine whether the slopes of gray matter vs. age were significantly different between groups.

We performed a voxelwise multiple regression analysis in SPM12 to identify regions in which preSxC9 and HC2 showed a differing correlation slope for the relationship between gray matter intensity and age. We reasoned that gray matter regions declining in excess of normal age-related volume changes, would be expected to show a significantly stronger negative correlation between gray matter intensity and age in carriers than controls.

2.4.1.2. Diffusion tensor imaging. Tract-Based Spatial Statistics analysis was performed in FSL (http://www.fmrib.ox.ac.uk/fsl) (Smith et al., 2006) (see Supplementary Methods: DTI preprocessing for details). Using a two-sample *t*-test via the general linear model framework in FSL, we compared group differences in fractional anisotropy (FA) maps of preSxC9 vs. HC3. Nuisance covariates included age, sex, handedness, education and TIV. The number of permutations was set at 5000. Significant clusters were defined at $p < 0.05$ corrected using the threshold-free cluster enhancement option. We chose to assess FA because it is the most stable, reliable and widely applied DTI metric, most optimal for selectively determining the directionality and microstructural integrity of white matter fibers (Pierpaoli and Basser, 1996). We extracted the mean FA within the preSxC9 < HC3 map (at pFWE < 0.05) for each participant and plotted the values versus age. We performed an ANCOVA to test for an interaction between age and gene status on FA, in order to determine whether the slopes of FA vs. age were significantly different between groups. We calculated a z-score of the mean FA within this preSxC9 < HC3 map and plotted the values versus age for visualization purposes only. Next, we probed for regions in which preSxC9 and HC3 showed a differing correlation slope for the relationship between FA and age.

2.4.1.3. Functional imaging. For preprocessing, the first 5 images were discarded to allow for magnetic field stabilization. Functional images were slice-time corrected, spatially realigned and unwarped (to reduce artifacts due to movement-by-deformation interactions), then coregistered to the subject's T1 image, normalized, and smoothed with a 6 mm full-width at half-maximum isotropic Gaussian kernel using SPM12. Each subject's T1 image was coregistered to the mean T2* image and normalized by calculating the warping parameters between the T1 image and the Montreal Neurological Institute T1 template and applying the parameters to all functional images in the sequence. Subsequently, images were re-sampled at a voxel size of 2 mm^3 and temporal bandpass filtered (0.008 to 0.15 Hz). To address residual motion and physiological artifacts, the following regressors were included in the first-level seed correlation analyses: the 6 rotational and translational motion parameters for each volume; the time series of deep white matter and cerebrospinal fluid regions of interest (ROIs); the temporal derivatives of the 8 resultant parameters to account for motion-related signal distortion in temporally adjacent volumes; and the squares of the 16 resultant parameters to account for quadratic trends. Following previous methods, we computed mean root-mean-square values of volume-to-volume changes in translational (in mm) and rotational (mean Euler angle) movement because these metrics correlate with network connectivity strength (Van Dijk et al., 2012). The 13 preSxC9 and 30 HC3 showed no differences in translation or rotational motion (Supplementary Table 3).

ROI analyses were conducted using 4 mm radius spherical seed regions employed in our previous work (Lee et al., 2014) to derive the 1) salience network, seeded at right ventral anterior insula [MNI coordinates 42, 17, −10] (Seeley et al., 2008); 2) SMN, seeded at right precentral gyrus [MNI coordinates 28, −16, 66] (Zielinski et al., 2010); and 3) default mode network (DMN), seeded at right angular gyrus [MNI coordinates 56, −52, 26] (Seeley et al., 2009). Since *C9ORF72*-bvFTD showed salience network disruption that correlated with gray matter atrophy in the left medial pulvinar thalamus (Lee et al., 2014), we further studied intrinsic functional connectivity to this region, whose peak voxel in the previous analysis was at MNI coordinates x = −9, y = −28, z = 3. Using the MARSBAR toolbox (Brett et al., 2002), we extracted the average blood oxygen level-dependent signal intensity of all voxels within a given seed throughout each participant's scan. For each scan, an ICN correlation map was produced in which each voxel contained the beta value of the seed ROI time series in the whole-brain regression analysis. Single-subject ICN correlation maps were then entered into a two-sample *t*-test via the general linear model framework in SPM12 to compare preSxC9 and HC3, with age, sex, education, and handedness included as nuisance regressors. Analyses were thresholded using joint probability distribution thresholding with a joint height and extent threshold of $p < 0.05$ corrected at the whole-brain level (Poline et al., 1997). Group salience network, SMN, and DMN maps were masked to the relevant ICN. ICN masks were derived from 15 independent healthy control participants using independent component analysis (Habas et al., 2009) and included subcortical regions and the cerebellum. Masks were thresholded at $t \geq 2.5$ to generously constrain the search volume for ICN contrasts, following previous methods (Lee et al., 2014), and are shown in Supplementary Fig. 1. Since a comparable ICN mask for medial pulvinar connectivity was not included in the study by Habas et al. (2009), unmasked results are shown. To illustrate the regions connected to the medial pulvinar in controls, we created a group map of 30 HC3 using a one sample *t*-test (Supplementary Fig. 2) thresholded at a joint height and extent threshold of $p < 0.0001$ corrected at the whole brain level (Poline et al., 1997). Using MARSBAR, we extracted the mean connectivity parameter estimates from within the preSxC9 vs. HC3 maps and plotted the values versus age for visualization purposes only. We performed an ANCOVA to test for an interaction between age and gene status on mean connectivity, in order to determine whether the slopes of mean connectivity vs. age were significantly different between groups. To seek accelerated connectivity disruption with advancing age, we searched for voxels in which preSxC9 showed a more negative correlation slope than HC3 for the relationship between intrinsic connectivity and age. To assess for potential effects of gray matter deficits on ICN strength, we used the Biological Parametric Mapping toolbox (Casanova et al., 2007) and entered each subject's VBM gray matter map as a set of voxelwise covariates in the regression model.

2.4.1.4. Neuroimaging w-score profiles. To compare single-subject data across neuroimaging modalities, we calculated w-scores for each preSxC9 for each modality. The gray matter w-score was calculated by extracting the gray matter intensity values within the preSxC9 < HC2 VBM map. We then performed a linear regression on the extracted HC2 gray matter values with age, sex, and TIV as covariates, and

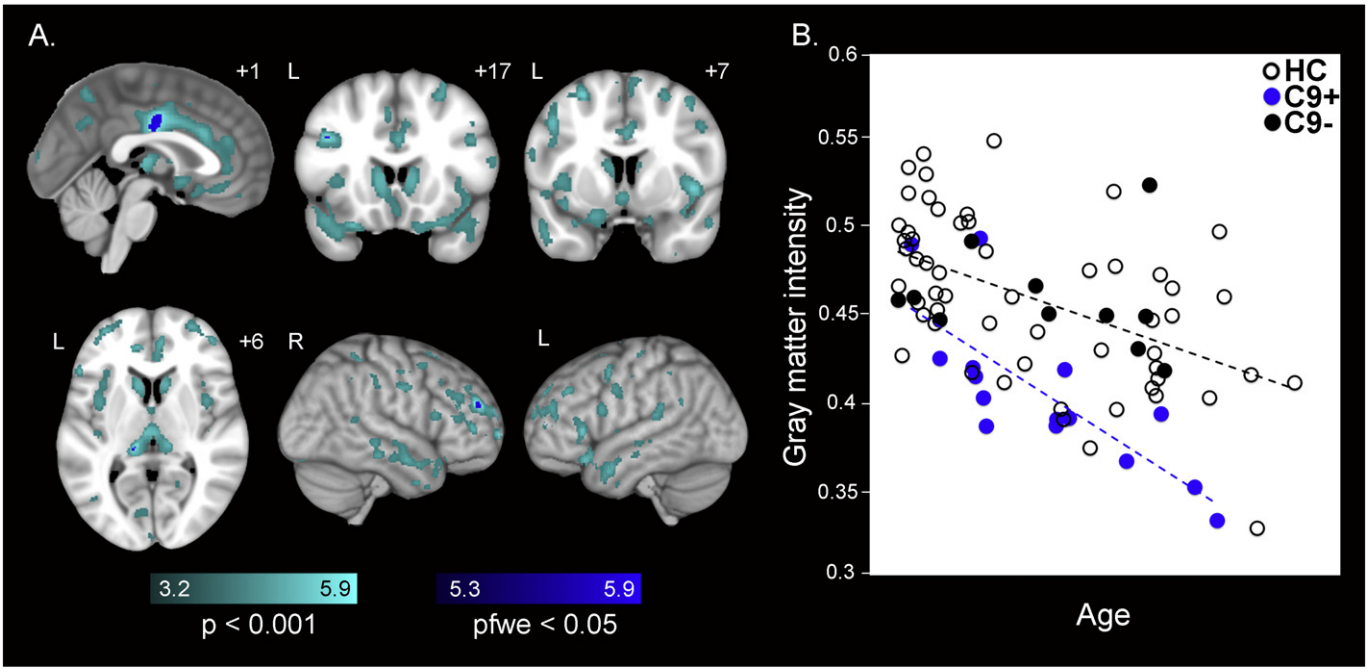

Fig. 1. Gray matter reductions in preSxC9. (A) Group difference maps derived using VBM illustrate reduced gray matter in 15 preSxC9 expansion carriers compared with 67 healthy controls (HC2) involving bilateral posterior midcingulate cortex, left medial pulvinar nucleus of the thalamus, and regions in bilateral dorsolateral prefrontal cortex at pFWE < 0.05 (dark blue). More extensive gray matter reductions in bilateral medial frontal cortex, dorsolateral prefrontal cortex, insula, precuneus and medial thalamus emerge at p < 0.001 uncorrected (cyan). Color bars represent t-scores, and statistical maps are superimposed on the Montreal Neurological Institute template brain. The left side of the axial and coronal images corresponds to the left side of the brain. (B) Mean gray matter intensity versus age within the pFWE < 0.05 map in (A), for 15 preSxC9 (blue dots), C9– (black dots), and HC (black circles) plotted for visualization purposes only. In general, preSxC9 showed lower gray matter intensities within the pFWE < 0.05 map in (A) compared with controls over three decades. Age axis labels are omitted to preserve subject anonymity. C9+ = presymptomatic *C9ORF72* expansion carriers; C9– = non-carrier family members; HC = non-family healthy controls. C9– and HC were combined to comprise HC2.

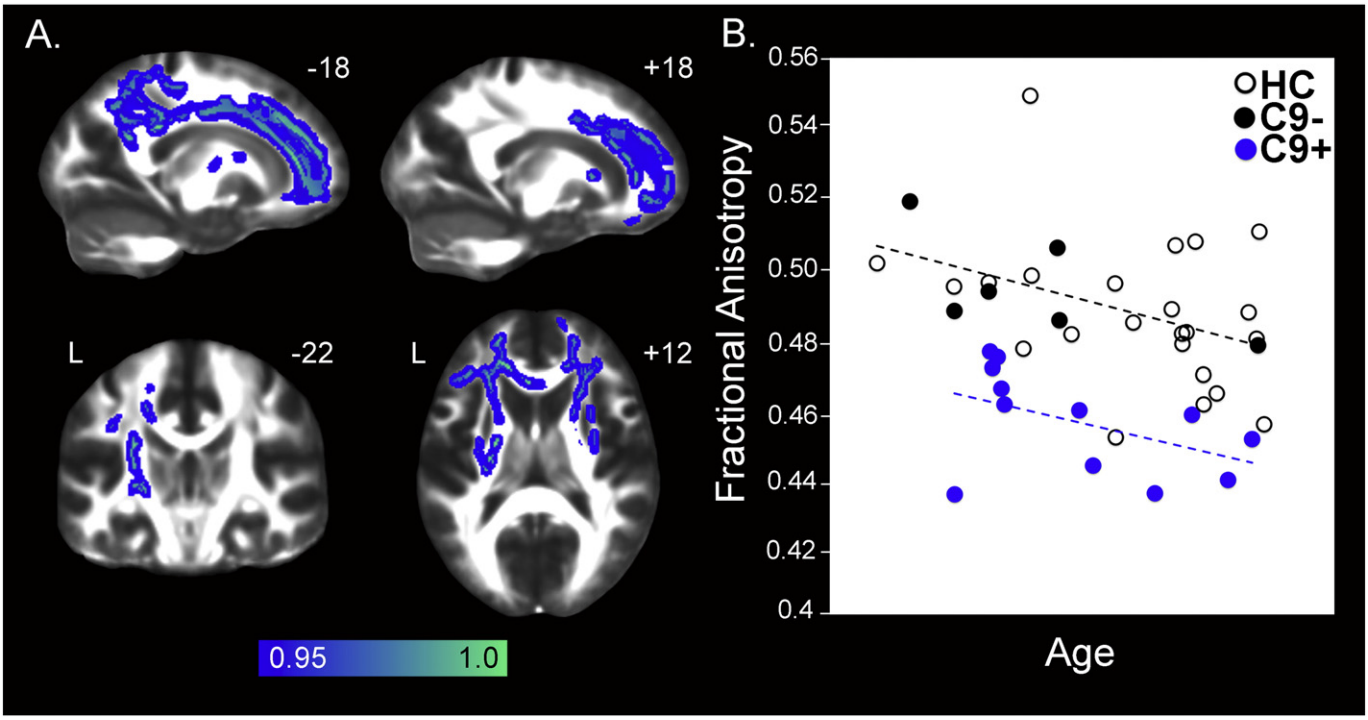

Fig. 2. Reduced white matter integrity in preSxC9. (A) Group difference FA maps show reduced fractional anisotropy in 12 preSxC9 compared with 29 healthy controls (HC3) including left greater than right cingulum bundle and corpus callosum and bilateral internal capsule at p < 0.05 corrected (blue-green). Color bars represent p values, and statistical maps are superimposed on the FMRIB58FA template. The left side of the axial and coronal images corresponds to the left side of the brain. (B) Mean FA versus age within the map in (A), for 12 preSxC9 (blue dots), C9– (black dots), and HC (black circles) plotted for visualization purposes only. PreSxC9 showed lower FA within the map in (A) compared with controls over three decades. Age axis labels are omitted to preserve subject anonymity. C9+ = presymptomatic *C9ORF72* expansion carriers; C9– = non-carrier family members; HC = non-family healthy controls. C9– and HC were combined to comprise HC3.

computed the unstandardized residuals in the regression model. The ICN w-scores for each subject were calculated by subtracting the predicted from the observed connectivity values, then dividing by the standard deviation of the HC2 residuals (w = observed – predicted / sd of healthy control residuals) (Jack et al., 1997). FA w-scores were calculated using an identical approach but based on the preSxC9 < HC3 DTI map.

Because preSxC9 subjects most often progress to bvFTD, bvFTD-MND, or ALS, we explored whether subjects might show varying degrees of connectivity disruption among the four ICNs, suggesting a prodromal state that might predispose to one clinical syndrome over others. To calculate w-scores representing ICN connectivity for each subject, we performed a one-sample *t*-test on the 30 HC3 single-subject ICN seed correlation maps. We thresholded the maps at a t-threshold = 6, in order to define regions that comprised the relevant ICN while minimizing overlap between ICNs. Next, we extracted the mean connectivity parameter estimate for each preSxC9 and HC3 subject within each ICN map, then performed a linear regression on the extracted mean connectivity parameter estimates with age and sex as covariates, then calculated ICN w-scores for each subject. A w-score composite was calculated by averaging three w-scores for each subject derived from the preSxC9 < healthy control difference maps for gray matter, fractional anisotropy and the mean connectivity beta value of the ICN showing the most reductions for that subject. We calculated the Cohen's d effect size based on w-scores of preSxC9 and controls for each imaging modality.

2.4.2. Screening for psychiatric and neurological history

A behavioral neurologist (S.E.L.) blinded to identifying subject data and mutation status performed a retrospective chart review of 15 preSxC9 carriers and 24 *C9ORF72*-family members. Specifically noted as present or absent in the record were: 1) psychiatric symptoms (ranging

Table 1
Demographic features and neuropsychological testing.

Demographic features and cognitive and behavioral battery	Healthy controls (n = 46)	Presymptomatic *C9ORF72* carriers (n = 15)	Test statistic, df	p
M:F, n	21:25	6:9	X = 0.15, 1	0.70
Handedness, L:R	6:40	2:13	X = 0.001, 1	0.98
Age at MRI scan, years	47.8 (11.2)	43.7 (10.2)	T = −1.25, 59	0.21
Education, years	15.9 (2.3)	16.1 (1.5)	U = 337	0.89
Mean familial age of onset, years	NA	51.8 (5.3)	NA	NA
Mean time to onset (based on mean familial age of onset), years	NA	8.2 (11.0)	NA	NA
CDR, total (median, range)	(0,0)	(0,0)	NA	NA
CDR, sum of boxes	0(0)	0(0)	NA	NA
Mini-Mental State Exam (max = 30)	29.2 (1.0)	29.0 (1.2)	U = 328	0.77
Memory				
California Verbal Learning Test, short form, four learning trials total (max = 36)	30.2 (3.4)	28.4 (2.7)	T = −1.83, 43	0.07
California Verbal Learning Test, short form, 10 min recall (max = 9)	7.9 (1.4)	6.9 (1.7)	U = 135.5	**0.04**
California Verbal Learning Test, total intrusions	0.2 (0.6)	1.2 (2.0)	U = 306	<**0.01**
Benson figure 10 min recall (max = 17)	12.8 (2.8)	12.3 (2.2)	U = 277.5	0.26
Visuospatial/calculations				
Benson figure copy (max = 17)	15.4 (1.0)	15.6 (1.4)	U = 386	0.47
Visual object and space perception battery (max = 10)	9.4 (1.0)	9.3 (1.0)	U = 306.5	0.54
Calculations (max = 5)	4.7 (0.5)	4.9 (0.4)	U = 382.5	0.38
Language/reading				
Abbreviated Boston naming test (max = 15)	14.2 (1.2)	13.4 (1.6)	U = 235	0.08
Wide range achievement test 4 (max = 70)	62.0 (4.7)	62.7 (2.8)	T = 0.47, 45	0.64
Executive				
Digit span forward	6.9 (1.1)	6.6 (1.2)	U = 227.5	0.28
Digit span backward	5.3 (1.5)	5.6 (1.2)	U = 360.5	0.49
Modified trails (correct lines per minute)	39.2 (17.8)	36.6 (18.6)	U = 304	0.50
Modified trails errors	0.5 (1.4)	0.3 (0.5)	U = 326	0.70
Stroop, color naming trial	94.2 (14.1)	91.7 (20.3)	T = −0.54, 56	0.59
Stroop, color naming trial errors	0.1 (0.3)	0.1 (0.4)	U = 349.5	0.28
Stroop, interference trial	55.4 (11.6)	55.4 (14.2)	T = −0.02, 54	0.99
Stroop, interference trial errors	0.4 (1.1)	0.0 (0.0)	U = 238	0.08
Letter fluency ('D' words in 1 min)	15.0 (4.4)	15.5 (4.2)	T = 0.33, 59	0.74
Semantic fluency (animals in 1 min)	23.2 (5.4)	21.0 (4.5)	T = −1.40, 59	0.17
Design fluency (correct designs per minute)	11.4 (3.5)	12.1 (3.7)	U = 359.5	0.71
Social/emotional				
Comprehensive affective testing system, face matching (max = 16)	11.8 (0.5)	11.7 (0.6)	U = 308	0.40
Comprehensive affective testing system, affect matching (max = 16)	13.2 (1.6)	12.6 (1.1)	U = 264.5	0.20
NPI frequency x severity (max = 144)	2.8 (4.0)	3.1 (5.8)	U = 192	0.94
Interpersonal Reactivity Index, fantasy	19.9 (6.1)	18.0 (5.3)	T = −0.85, 32	0.40
Interpersonal Reactivity Index, empathic concern	28.1 (5.7)	28.5 (4.7)	U = 114.5	0.85
Interpersonal Reactivity Index, perspective taking	24.0 (5.5)	22.4 (6.0)	T = −0.73, 32	0.47
Interpersonal Reactivity Index, personal distress	12.2 (4.0)	14.9 (7.5)	T = 1.39, 32	0.17
Geriatric depression scale (max = 30)	3.2 (3.5)	4.5 (6.1)	U = 329	0.91

Abbreviations: df = degrees of freedom; NA = not applicable.

from self-report to psychiatric conditions diagnosed by a medical professional), 2) a history of psychiatric or psychological treatment, i.e. consultation with a psychiatrist or a psychologist, but not necessarily needing inpatient hospitalization or medications for psychiatric indications 3) medications taken for psychiatric indications, 4) psychiatric hospitalizations, 5) prolonged substance use or abuse, and 6) childhood neurological developmental disorder (dyslexia, speech problems, attention deficit hyperactivity disorder). Importantly, clinicians eliciting these data points at the time of clinical history were also blinded to subjects' genetic status.

2.4.3. Statistical analysis

We compared clinical variables and TIV using the chi-squared test, *t*-test or Mann-Whitney U as appropriate. Test statistics were considered significant at $p < 0.05$ (two-tailed).

3. Results

3.1. PreSxC9 show preserved social-emotional-cognitive function despite structural brain deficits and reduced intrinsic network connectivity

By design, preSxC9 and HC1 were well-matched for demographic characteristics (Table 1). On neuropsychological measures, preSxC9 showed lower scores on the California Verbal Learning Test ten minute recall ($p = 0.04$) and had more intrusions across all trials ($p < 0.01$). All other neuropsychological tests showed similar scores in both groups. In preSxC9, estimated time to symptom onset showed a strong negative correlation with age (Pearson $r = -0.88$, $p < 0.01$). Among the preSxC9, the clinical syndromes seen among their 96 symptomatic family members included: bvFTD 31%, ALS 27%, FTD-MND 17%, AD-like 12%, and unspecified dementia 13%.

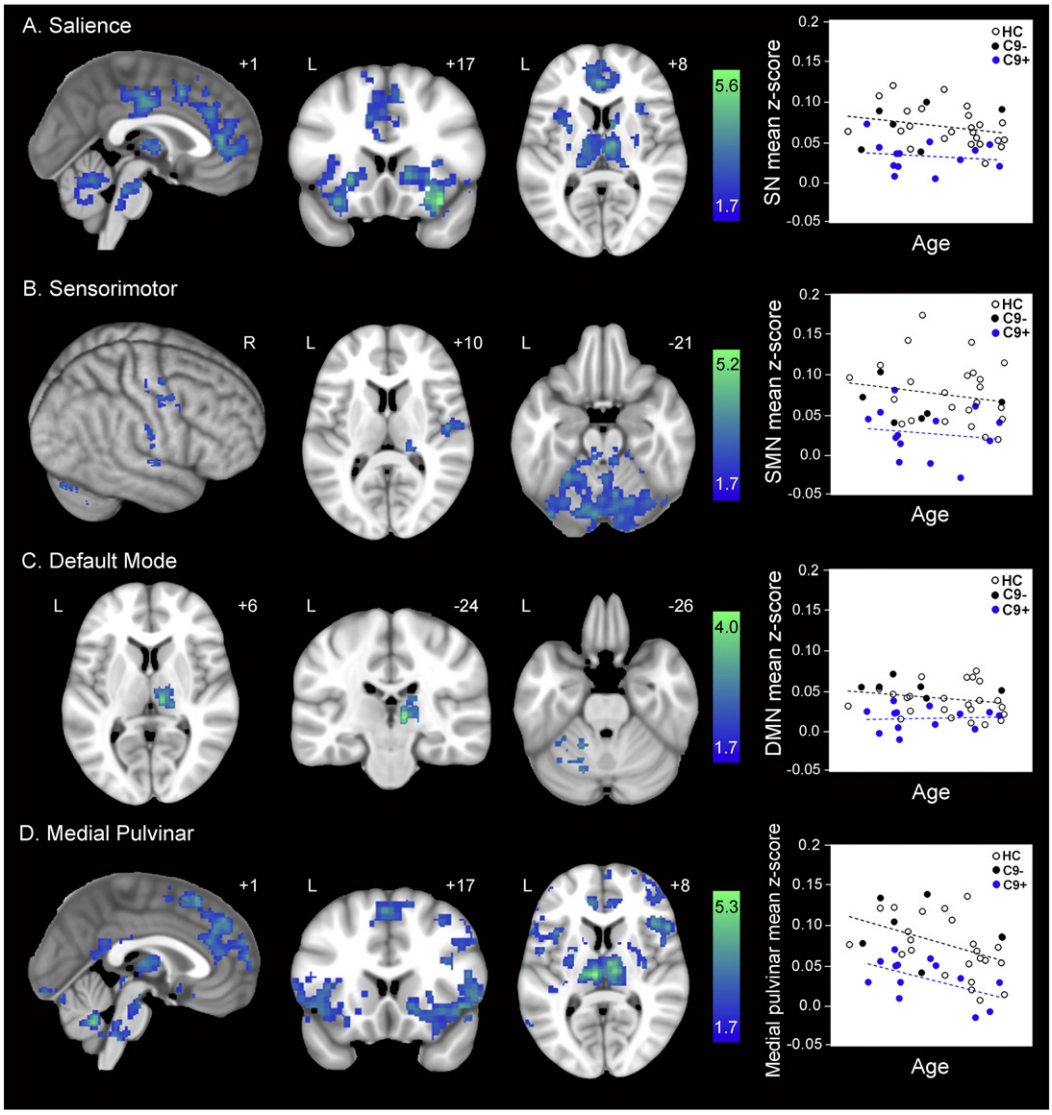

Fig. 3. ICN reductions in preSxC9. Group difference maps show reduced intrinsic connectivity in 13 preSxC9 compared with 30 healthy controls (HC3) for all four networks studied: (A) salience network; (B) SMN; (C) DMN; and (D) medial pulvinar. Note the topographic similarity of connectivity reductions in the salience network (A) and medial pulvinar network (D). Analyses were thresholded using joint probability distribution thresholding with a joint height and extent threshold of $p < 0.05$ corrected at the whole-brain level. Color bars represent t-scores, and statistical maps are on the Montreal Neurological Institute template brain. The left side of the axial and coronal images corresponds to the left side of the brain. Mean ICN parameter estimate versus age within the maps at left are plotted for 13 preSxC9 (blue dots), C9– (black dots), and HC (black circles). All four plots suggest ICN reductions throughout the age span studied. Age axis labels are omitted to preserve subject anonymity. C9+ = presymptomatic *C9ORF72* expansion carriers; C9– = non-carrier family members (black dots); HC = non-family healthy controls. C9– and HC were combined to comprise HC3.

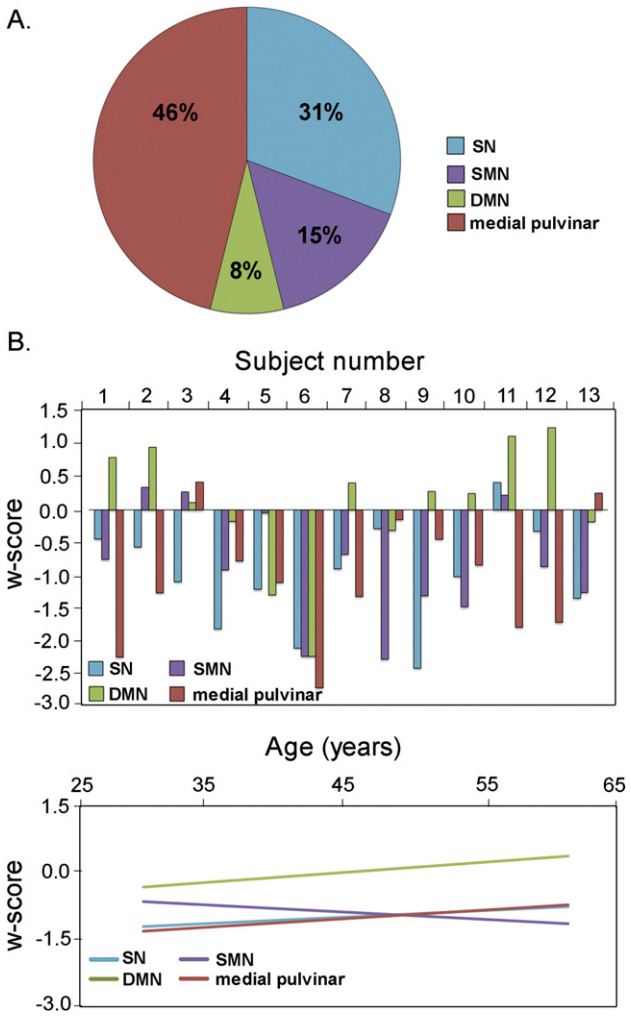

Fig. 4. Salience and medial pulvinar connectivity disruptions predominate in preSxC9. In (A), the pie chart shows the percentage of preSxC9 participants in whom the salience network (blue), SMN (purple), DMN (green), or medial pulvinar connectivity (red) was the ICN with the lowest connectivity w-score among the four ICNs. (B) w-scores of mean connectivity reveal that 13 preSxC9 show heterogeneous ICN reduction profiles, with salience and medial pulvinar networks showing most disruption across the age span. Subjects are ordered by ascending age. (C) Fit-lines of the w-scores in B show that salience and medial pulvinar connectivity are the lowest throughout the presymptomatic phase.

Compared to HC2, preSxC9 showed lower gray matter intensity in bilateral posterior mid-cingulate, left medial pulvinar thalamus, and small, scattered regions in bilateral dorsolateral prefrontal cortex ($pFWE < 0.05$; Fig. 1A and Supplementary Table 4). At a more lenient statistical threshold ($p < 0.001$ uncorrected), more extensive gray matter deficits were seen, involving bilateral anterior cingulate, medial frontal regions, insula, frontal pole, temporal pole, dorsolateral prefrontal cortex, precentral gyrus, precuneus, occipital cortex, striatum, and medial thalamus. Notably, preSxC9 showed no gray matter reductions in the cerebellum, even at this more lenient statistical threshold. As expected, no regions showed higher gray matter intensity in preSxC9 than HC2 at either threshold.

PreSxC9 showed reduced white matter integrity, as assessed by FA, more extensive in left greater than right corpus callosum and cingulum bundle. Other tracts showing reduced FA included bilateral internal and external capsule (Fig. 2A and Supplementary Table 5). No white matter tracts showed higher FA in preSxC9 than HC3.

In task-free fMRI analyses, preSxC9 showed intrinsic connectivity deficits in all four ICNs and no enhancements compared to controls. In the salience network, reduced connectivity to the right frontoinsula was widespread, appearing in bilateral anterior and mid-cingulate cortex, anterior insula, striatum, thalamus, pons and cerebellum (Fig. 3A), strongly resembling the pattern of salience network disruptions seen in *C9ORF72*-bvFTD (Lee et al., 2014). SMN connectivity reductions to the right precentral gyrus were detected in right pre- and post-central gyrus, right thalamus, and bilateral pons and cerebellum (Fig. 3B). DMN connectivity reductions to the right angular gyrus were absent throughout the cerebral cortex but were seen in the right thalamus and left cerebellum (Fig. 3C). Connectivity to the medial pulvinar thalamus was widely disrupted, with disconnections in bilateral ACC/medial frontal cortex, dorsolateral prefrontal cortex, anterior insula, striatum, anterior thalamus, brainstem and cerebellum (Fig. 3D), mirroring the observed salience network reductions (Fig. 3A). Adjusting the ICN comparisons for gray matter intensity yielded similar results, suggesting that ICN reductions in preSxC9 cannot be attributed to gray matter deficits (Supplementary Table 6). For both the gray matter adjusted and unadjusted analyses, no network showed intrinsic connectivity enhancements in preSxC9.

Among the 13 preSxC9 participants, most showed the medial pulvinar-seeded network (46%) or salience network (31%) as the most disrupted ICN examined (Fig. 4A). Overall, the salience network, SMN, and medial pulvinar network w-scores were less than zero for nearly all subjects, but individual carriers showed contrasting patterns of ICN vulnerability (Fig. 4B). Fit lines of these w-scores vs. age suggest that salience and medial pulvinar network connectivity is impaired early, in the range of $w = -1.5$ to -1.0 and remains low throughout the presymptomatic phase. Two preSxC9 showed the SMN as the most disrupted network. For these preSxC9 whose SMN was the most disrupted ICN, subject 8, aged in the mid-forties, also had mildly low precentral gyrus volumes on the left ($w = -1.24$) and right ($w = -1.18$), but interestingly, Subject 10, with an age in the early fifties had very low gray matter for age in the left precentral gyrus ($w = -2.26$) but not the right ($w = -1.66$). Though less affected than the other two networks, SMN showed a slight decline with age, while DMN remained at stable levels throughout the age span.

3.2. Brain structural and functional deficits in preSxC9 show no acceleration with advancing age

We considered two possible explanations for the observed preSxC9 gray matter volume deficits and brain connectivity disruptions: incipient neurodegeneration and abnormal brain development. Incipient neurodegeneration, our leading hypothesis, would be expected to produce accelerating deficits as carriers approach predicted symptom onset. Abnormal brain development, on the other hand, should be detectable across the adult age span. Although these explanations are not mutually exclusive, to provide a preliminary evaluation of these models we extracted the mean gray matter intensities within the maps representing the preSxC9 < HC2 contrast ($pFWE < 0.05$ and $p < 0.001$ uncorrected). Plotting this value against age revealed that, contrary to our lead hypothesis, preSxC9 showed lower gray matter intensity across three decades, including subjects in their early thirties (Fig. 1B). Across this age span, gray matter intensities in preSxC9 showed a similar relationship to age as seen in HC2, with the exception of two carriers whose values fell within the control range. Similarly, when we plotted each subject's FA (Fig. 2B) and mean ICN scores (Fig. 3) derived from their respective preSxC9 < HC3 maps, we found that reduced white matter integrity and connectivity in all four ICNs again appeared during the early thirties with mean values showing a similar relationship to age as seen in controls. There were no significant differences between the slopes of preSxC9 and HC for gray matter vs. age ($p = 0.22$), for FA vs. age ($p = 0.89$), or for mean connectivity vs. age (salience network $p = 0.70$; SMN $p = 0.85$; DMN $p = 0.40$; medial

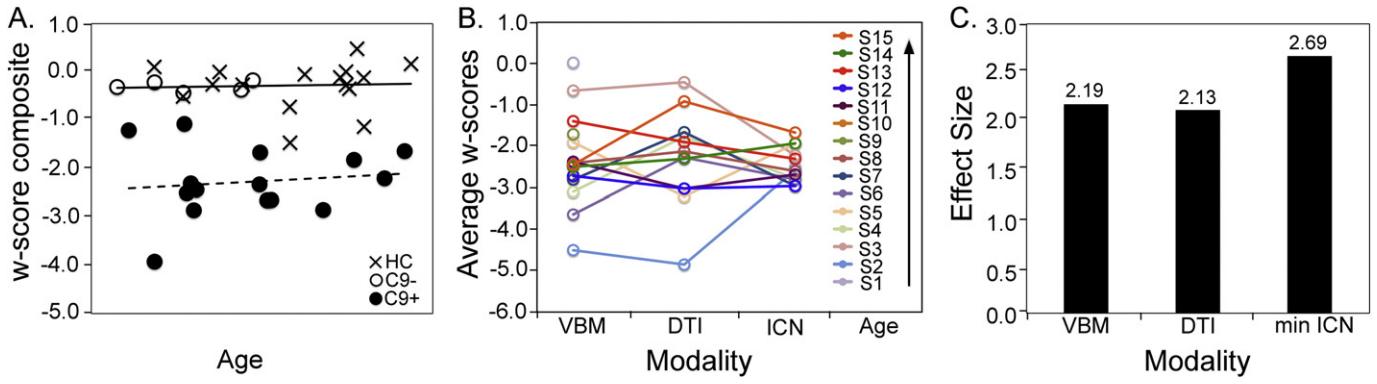

Fig. 5. Multimodal imaging composite scores separate preSxC9 from controls and show structural and functional connectivity disruption as early as the third decade. (A) The plot shows a w-score composite (the average of gray matter intensity, fractional anisotropy and lowest ICN w-scores for each subject) plotted versus age. The C9+ fit line appears horizontal, thus suggesting a consistently reduced w-score composite across the entire age range. (B) Individual C9+ subject w-scores from VBM, DTI, and ICN analyses for the most reduced ICN for each subject in order of ascending age. (C) Effect size (Cohen's d) for detecting differences between C9+ and controls for VBM, DTI, and most reduced (weakest) ICN. C9+ = presymptomatic *C9ORF72* expansion carriers (black dots); C9– = non-carrier family members (black circles); HC = healthy controls included in all three imaging modalities (indicated by "x"). Axis labels for age were omitted to preserve anonymity.

pulvinar network $p = 0.86$). Thus, results across three imaging modalities provide converging evidence that brain structure and function abnormalities arise early in preSxC9, reflecting either neurodevelopmental differences or a protracted course of neurodegeneration that begins in early adulthood but smolders over several decades before symptoms emerge.

To more formally assess whether brain structure and function abnormalities accelerate as preSxC9 subjects near symptom onset, we performed a voxelwise analysis to seek out brain regions in which imaging metrics showed a more negative correlation with age in preSxC9 than in controls. Consistent with our inspection of the mean gray matter intensity vs. age relationship (Fig. 1B), we found no region within the preSxC9 < HC2 pattern (Fig. 1A) showing a stronger decline with age in carriers than controls at either $p < 0.001$ uncorrected or $pFWE < 0.05$.

Similar voxelwise analyses of FA or ICN connectivity also showed no regions in which a more negative correlation with age emerged in preSxC9 than in controls. The w-score composite combines indices of gray matter intensity and fractional anisotropy within significantly reduced regions in preSxC9 as well as the most disrupted ICN network for each subject (Fig. 5a) and adjusts these values for covariates of no interest. All preSxC9 show a w-score composite less than −1, with more negative w-scores representing more deficits, and subjects showed consistently low w-score composites across four decades. The Cohen's d effect sizes were similar across all imaging modalities (Fig. 5c). Although longitudinal data are needed, these cross-sectional findings suggest that preSxC9 structural and functional connectivity deficits do not accelerate with age during the presymptomatic phase.

3.3. PreSxC9 and their C9ORF72-family members show similar psychiatric histories

Given the reported prevalence of psychosis in *C9ORF72*-bvFTD, we hypothesized that psychiatric symptoms might represent a prodromal manifestation of the structural and functional brain abnormalities observed in presymptomatic carriers. To test this idea, we compared lifetime prevalence of psychiatric disease in the 15 preSxC9 to their 24 *C9ORF72*-family members. The groups had similar age, sex, handedness, and education (Supplementary Table 7). Consistent with our hypothesis, preSxC9 showed high rates of psychiatric disease including psychiatric symptoms (47%), seeking professional psychiatric or psychological treatment (33%), taking medications for psychiatric indications (20%), psychiatric hospitalizations (7%), prolonged substance use or abuse (27%), and childhood neurological developmental disorders (7%). Contrary to our hypothesis, however, non-carrier family members showed a similarly high burden of psychiatric disease. In fact, the percentage of non-carrier family members taking psychiatric medications was nearly double that seen in preSxC9, although this difference did not reach statistical significance due to the relatively small sample sizes (Fig. 6, $p = 0.25$).

4. Discussion

Neurodegenerative disease-causing mutations, although present from conception, typically cause clinical symptoms only in mid-to-late life. Here, we sought insights into this mystery by asking whether and how the *C9ORF72* expansion impacts brain structure and function across the four to five decades of adult life that precede symptom onset. Expansion carriers showed structural and functional deficits within regions and networks known to become atrophied and disconnected in symptomatic *C9ORF72*-associated bvFTD and ALS. From one perspective, these preSxC9 deficits may represent the earliest stages of neurodegeneration. Another possibility is that these deficits reflect an abnormal neurodevelopmental trajectory. This alternative model is important to consider because a neurodevelopmental contribution to

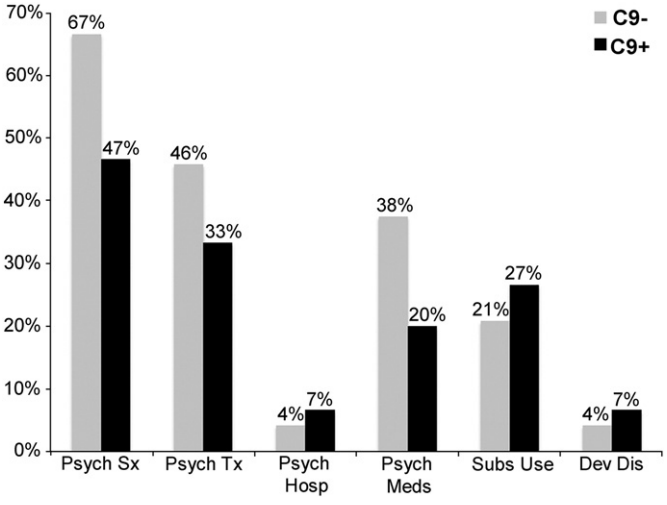

Fig. 6. Psychiatric histories in preSxC9 and *C9ORF72* family members negative for the expansion. No statistically significant differences emerged in preSxC9 (C9+, black bars, N = 15) versus their expansion-negative family members (C9−, gray bars, N = 24) for psychiatric symptoms (Psych Sx), psychiatric or psychological treatment (Psych Tx), psychiatric medications (Psych Meds), psychiatric hospitalizations (Psych Hosp), prolonged substance use or abuse (Subs Use), or childhood neurological developmental disorders (Dev Dis).

pathogenesis would have major implications for how we conceptualize, monitor, and treat inherited neurodegeneration.

Although preSxC9 individuals showed structural and functional deficit patterns that mirrored the symptomatic phase, to our surprise, these deficits were detectable by the fourth decade of life with no acceleration in older subjects presumably closer to symptom onset. Furthermore, because we could not pinpoint an associated cognitive, behavioral or psychiatric profile, the brain abnormalities identified appear to represent a compensated lesion, whether developmental or degenerative. Taken together, our findings from three complementary imaging modalities suggest that focal gray matter, structural connectivity, and functional connectivity deficits in preSxC9, whatever their nature, emerge no later than early adulthood and may set the stage for neurodegeneration during the symptomatic phase.

4.1. Structural and brain connectivity deficits occur in preSxC9 without apparent functional consequences

PreSxC9 individuals are at risk for bvFTD, ALS, or both, yet the pattern of gray matter volume deficits detected here largely recapitulates the regional pattern observed in *C9ORF72*-bvFTD, including the medial pulvinar region where there is accentuated atrophy in *C9ORF72*-bvFTD vs. sporadic bvFTD (Lee et al., 2014). Notably, *C9ORF72*-ALS shows more prominent frontal, anterior cingulate, thalamic (Bede et al., 2013; Cistaro et al., 2014) and precentral gyrus involvement (Byrne et al., 2012) than does sporadic ALS, suggesting that fronto-cingulo-thalamic degeneration and dysfunction are shared across *C9ORF72*-associated syndromes. Moreover, the imaging techniques employed here are better suited to examine bvFTD-vulnerable regions than ALS-vulnerable lower motor neuron-containing regions in the pons, medulla, and spinal cord. One previous study suggested that preSxC9 may show reduced gray matter in thalamus, hippocampus, insula, and parieto-occipital cortex, up to 25 years before onset (Rohrer et al., 2015). Our data further develop the picture by virtue of the voxelwise nature of our analyses. This approach, which provides a comprehensive assessment of brain structure unbiased by region-of-interest parcellation, identified the medial pulvinar of the thalamus as the area with the most prominent gray matter deficit.

We identified preSxC9-associated white matter deficits in tracts thought to degenerate in *C9ORF72*-bvFTD and -ALS. To date, studies of white matter deficits in *C9ORF72*-bvFTD involve limited sample sizes (Mahoney et al., 2014); in ALS with or without *C9ORF72*, affected tracts include the corpus callosum and the superior corticospinal tract. *C9ORF72*-ALS shows additional damage in frontotemporal tracts, the genu of the corpus callosum, the anterior commissure and bilateral thalami (Bede et al., 2013). In contrast to our findings, a previous study comparing preSxC9 and controls showed no differences in white matter tract integrity (Walhout et al., 2015). Several explanations may account for these differences between studies. First, subjects in the study by Walhout and colleagues were from the same kindred, whose mean familial time to onset was later than that of the subjects in the present study. Second, our larger control sample size provided greater statistical power to detect group differences. Third, instead of choosing specific tracts for tractography, we used a whole-brain voxelwise approach to DTI analyses. As with the gray matter deficits, preSxC9 reductions in white matter integrity emerged in the early thirties without apparent acceleration in older subjects more likely to approach symptom onset.

In concert with structural deficits, preSxC9 showed reduced connectivity within functional networks disrupted in *C9ORF72*-bvFTD (Lee et al., 2014). The salience network, a focus of network-based degeneration in bvFTD (Seeley et al., 2009, 2007) and *C9ORF72*-bvFTD, showed extensive preSxC9 reductions in bilateral anterior insula and anterior cingulate, as well as striatum, thalamus, and brainstem. Although sporadic and *C9ORF72*-bvFTD show comparable salience network disruption, medial pulvinar degeneration in *C9ORF72*-bvFTD correlates with and may drive salience network disconnection as a “strategic lesion” (Lee et al., 2014). Consistent with this model, reduced connectivity in preSxC9 was detected between the medial pulvinar thalamus and regions remarkably similar to those disconnected from the right frontoinsula (salience network) seed. The medial pulvinar, an association nucleus that participates in cortico-cortical interactions, helps to guide visual attention by detecting salient environmental stimuli (Benarroch, 2015). In the rhesus monkey, the medial pulvinar shows extensive connections with the insula and high order polymodal association cortex (Mufson and Mesulam, 1984), and superior temporal gyrus and sulcus, anterior and posterior cingulate and amygdala (Romanski et al., 1997). Several studies suggest a role for the medial pulvinar in processing human facial emotion (Maior et al., 2010) and rapid detection of biological threats (Van Le et al., 2013). All but three carriers showed the greatest degree of disruption in the salience and medial pulvinar-seeded networks, suggesting that these networks are impacted early and extensively in preSxC9. Although we found no symptomatic or neuropsychological correlate of the widespread structural and functional connectivity deficits in preSxC9, systematic laboratory-based or targeted questionnaire-based studies may elucidate subclinical impairments.

The carriers in the present study showed MND in 44% of their affected kin, alone or in combination with bvFTD. In parallel with our work in *C9ORF72*-bvFTD (Lee et al., 2014), our findings showed preSxC9 disruptions in key SMN nodes, including primary motor and somatosensory cortex and cerebellum, again with vulnerability starting in the early thirties. Two possibilities are that all preSxC9 harbor SMN vulnerability, whether or not a given carrier will develop clinical MND, or that individual preSxC9 show differential SMN vulnerability that will predict future MND. At the group level, preSxC9 showed SMN deficits despite no upper or lower motor neuron signs on examination. Longitudinal follow-up will determine whether the two preSxC9 whose SMN w-scores were the most reduced among the four ICNs will develop clinical MND.

In our previous work, *C9ORF72*-bvFTD demonstrated similar DMN connectivity to controls, yet individual carriers with mild or slowly progressive disease showed DMN connectivity enhancements, similar to those seen in sporadic bvFTD (Farb et al., 2013; Zhou et al., 2010). Thus, we hypothesized that preSxC9, like mildly symptomatic carriers, might show DMN enhancements that would subside during the early symptomatic phase. Contrary to our hypothesis, we found focal DMN reductions in the thalamus and cerebellum, rather than in canonical DMN cortical regions, but no enhancements, suggesting that DMN connectivity may exhibit greater instability (from weakened to intensified) across the natural history of *C9ORF72* disease. Moreover, we found that individual subjects showed heterogeneous vulnerability profiles across the four ICNs studied. Thus, as with any group analysis, individual subject variability may also be obscured, underlining the importance of mapping longitudinal intra-subject connectivity trajectories.

4.2. Structural deficits and C9ORF72-related network connectivity disruption in preSxC9 may represent a developmental lesion rather than early neurodegeneration

We found that preSxC9 showed gray and white matter deficits and ICN disruption as early as the fourth decade of life and that these deficits exhibited no accentuation in older carriers nearer to predicted age of symptom onset. Two young preSxC9 showed gray matter volumes within the range of healthy controls, raising the question of whether the gray matter deficits in the remaining carriers represented early atrophy. Adjusted for age, connectivity in all four ICNs also showed disruptions during the fourth decade and remained consistently reduced throughout the age span studied with no worsening in older carriers.

Regions within the preSxC9 gray matter, white matter, or ICN deficit patterns showed no more pronounced age-related decline

than seen in the healthy aging trajectories. These findings raise the intriguing possibility that the structural and functional deficits represent the result of abnormal brain development. Although the function of the *C9ORF72* protein remains uncertain, decreased *C9ORF72* mRNA expression leading to the loss of *C9ORF72* protein function is a potential pathogenic mechanism (DeJesus-Hernandez et al., 2011). Since human brain *C9ORF72* expression is known to emerge as early as eight weeks post-conception (Miller et al., 2014), altered expression may impact brain development. Mice lacking *C9ORF72* exhibit a neuroinflammatory phenotype, with age-related microglial dysfunction (O'Rourke et al., 2016) that has been proposed to augment the neurodegenerative process. Microglia are also crucial players in brain development, however, and the early-life brain structure and function deficits shown here could be linked to loss of *C9ORF72* function via an over-pruning of synapses by overactive microglia. Alternatively, repeat-containing RNA foci and dipeptide repeat protein inclusions could emerge during the presymptomatic phase, at least in some individuals (Proudfoot et al., 2014; Vatsavayai et al., n.d.), and impact neurodevelopment or create a protracted phase of smoldering decline before a second pathogenic event leads to accelerated neurodegeneration.

Although previous studies have not systematically investigated developmental differences in *C9ORF72*, scattered reports of *C9ORF72* expansion carriers with intellectual disabilities have come to light. One report described a *C9ORF72* kindred including two individuals with childhood intellectual disabilities (Proudfoot et al., 2014). One man requiring special education was confirmed to carry the *C9ORF72* expansion and died of pulmonary embolism at age 26 without clinical FTD or ALS; his autopsy showed widespread dipeptide repeat protein inclusions. Another *C9ORF72* expansion carrier with normal early development showed learning difficulties at age six requiring special education (Hensman Moss et al., 2014). Among our 15 preSxC9 and 24 *C9ORF72*-, only one subject from each group showed a childhood neurological developmental disorder (Fig. 3), suggesting that severe childhood intellectual or developmental disorders are not a common feature of *C9ORF72* despite the brain structure and function deficits apparent in early adulthood. Studying preSxC9 during childhood and early adulthood will be required to clarify the nature of the early adulthood preSxC9 changes and their biological basis, as has been done with infants carrying the apolipoprotein E4 gene, a risk factor for Alzheimer's disease, who show differences in brain structure compared to E4 non-carriers (Dean et al., 2014).

4.3. PreSxC9 and their non-carrier family members share psychiatric symptomatology

Could psychiatric symptoms in preSxC9 represent a clinical prodrome and herald bvFTD? Several series have reported a higher incidence of psychosis in *C9ORF72*-associated than sporadic bvFTD (Boeve et al., 2012; Majounie et al., 2012; Snowden et al., 2012). Patients with typical bipolar disorder and schizophrenia show gray matter deficits in regions that degenerate in bvFTD, including the anterior cingulate, bilateral frontoinsula (Bora et al., 2010), temporal pole and medial frontal cortex (Gupta et al., 2014). These considerations prompted us to hypothesize that structural deficits in preSxC9 might be associated with a *C9ORF72*-specific psychiatric prodrome. Contrary to our hypothesis, preSxC9 and non-carrier family members showed similar rates of psychiatric disease ranging from self-reported symptoms to psychiatric hospitalization. In the general population, lifetime prevalence of psychiatric disorders is common: one survey showed that nearly 50% of the non-institutionalized civilian United States population reported at least one lifetime psychiatric disorder (Kessler et al., 1994). Risk for psychiatric disease is enhanced by major life stressors, an unavoidable reality for preSxC9 dealing with neurodegenerative disease in their families and the uncertainties surrounding their own future neurological health. Our negative results should be considered with caution, however. The NPI was designed to capture twelve behavioral disturbances common in patients with dementia and could be less sensitive to changes in a non-demented cohort. Measures tailored for presymptomatic FTD mutation carriers may prove more sensitive to subtle symptoms that relate to the pattern of structural and functional deficits seen here and in studies of other genetic cohorts (Dopper et al., 2014; Whitwell et al., 2011).

4.4. Limitations and future directions

The study's limitations include the relatively small sample of preSxC9 and the cross-sectional design. The sample size may have limited power to detect more subtle between-group differences, especially with regard to psychiatric symptoms and brain-behavior correlations. Although our preSxC9 sample size was comparable to previous studies (Rohrer et al., 2015; Walhout et al., 2015), we increased statistical power by including a large healthy control group in our imaging analyses. To determine whether the structural and functional deficits in preSxC9 represent developmental versus degenerative changes will require a larger sample size with a longitudinal design and earlier life assessments to characterize individualized trajectories. Following carriers throughout the disease course will determine whether these deficits accelerate at an inflection point or must merely exceed a critical threshold. Clarifying the nature and time course of brain structure and function changes in presymptomatic inherited FTD remains a critical goal for understanding disease pathogenesis and for designing clinical trials.

Funding

This work was supported by the National Institutes of Health [SEL: K23AG039414, TPZ: F32AG030249, R01MH096861, GC: AG035610, BLM: P01AG019724; P50AG23501, WWS: AG023501, AG19724]; the John Douglas French Alzheimer's Foundation [GC]. Samples from the National Cell Repository for Alzheimer's Disease (NCRAD), which receives government support under a cooperative agreement grant (U24AG21886) awarded by the National Institute on Aging (NIA), were used in this study.

Acknowledgments

We thank contributors who collected samples used in this study, as well as patients and their families, whose help and participation made this work possible. We would like to thank Renaud La Joie for his valuable input.

Appendix A. Supplementary data

Supplementary data to this article can be found online at http://dx.doi.org/10.1016/j.nicl.2016.12.006.

References

Beckmann, C.F., DeLuca, M., Devlin, J.T., Smith, S.M., 2005. Investigations into resting-state connectivity using independent component analysis. Philos. Trans. R. Soc. Lond. Ser. B Biol. Sci. 360:1001–1013. http://dx.doi.org/10.1098/rstb.2005.1634.

Bede, P., Bokde, A.L.W., Byrne, S., Elamin, M., McLaughlin, R.L., Kenna, K., Fagan, A.J., Pender, N., Bradley, D.G., Hardiman, O., 2013. Multiparametric MRI study of ALS stratified for the C9orf72 genotype. Neurology 81:361–369. http://dx.doi.org/10.1212/WNL.0b013e31829c5eee.

Benarroch, E.E., 2015. Pulvinar: associative role in cortical function and clinical correlations. Neurology 84:738–747. http://dx.doi.org/10.1212/WNL.0000000000001276.

Boeve, B.F., Boylan, K.B., Graff-Radford, N.R., DeJesus-Hernandez, M., Knopman, D.S., Pedraza, O., Vemuri, P., Jones, D., Lowe, V., Murray, M.E., Dickson, D.W., Josephs, K.A., Rush, B.K., Machulda, M.M., Fields, J.A., Ferman, T.J., Baker, M., Rutherford, N.J., Adamson, J., Wszolek, Z.K., Adeli, A., Savica, R., Boot, B., Kuntz, K.M., Gavrilova, R., Reeves, A., Whitwell, J., Kantarci, K., Jack, C.R., Parisi, J.E., Lucas, J.A., Petersen, R.C., Rademakers, R., 2012. Characterization of frontotemporal dementia and/or amyotrophic lateral sclerosis associated with the GGGGCC repeat expansion in C9ORF72. Brain 135:765–783. http://dx.doi.org/10.1093/brain/aws004.

Bora, E., Fornito, A., Yücel, M., Pantelis, C., 2010. Voxelwise Meta-Analysis of Gray Matter Abnormalities in Bipolar Disorder. 67. BPS:pp. 1097–1105. http://dx.doi.org/10.1016/j.biopsych.2010.01.020.

Brett, M., Anton, J.-L., Valabregue, R., Poline, J.-B., 2002. Region of interest analysis using an SPM toolbox [abstract]. Presented at the Presented at the 8th International Conference on Functional Mapping of the Human Brain, June 2–6, 2002, Sendai, Japan.

Byrne, S., Elamin, M., Bede, P., Shatunov, A., Walsh, C., Corr, B., Heverin, M., Jordan, N., Kenna, K., Lynch, C., McLaughlin, R.L., Iyer, P.M., O'Brien, C., Phukan, J., Wynne, B., Bokde, A.L., Bradley, D.G., Pender, N., Al-Chalabi, A., Hardiman, O., 2012. Cognitive and clinical characteristics of patients with amyotrophic lateral sclerosis carrying a C9orf72 repeat expansion: a population-based cohort study. Lancet Neurol. 11: 232–240. http://dx.doi.org/10.1016/S1474-4422(12)70014-5.

Casanova, R., Srikanth, R., Baer, A., Laurienti, P.J., Burdette, J.H., Hayasaka, S., Flowers, L., Wood, F., Maldjian, J.A., 2007. Biological parametric mapping: a statistical toolbox for multimodality brain image analysis. NeuroImage 34:137–143. http://dx.doi.org/10.1016/j.neuroimage.2006.09.011.

Cistaro, A., Pagani, M., Montuschi, A., Calvo, A., Moglia, C., Canosa, A., Restagno, G., Brunetti, M., Traynor, B.J., Nobili, F., Carrara, G., Fania, P., Lopiano, L., Valentini, M.C., Chiò, A., 2014. The metabolic signature of C9ORF72-related ALS: FDG PET comparison with nonmutated patients. Eur. J. Nucl. Med. Mol. Imaging 41:844–852. http://dx.doi.org/10.1007/s00259-013-2667-5.

Cummings, J.L., Mega, M., Gray, K., Rosenberg-Thompson, S., Carusi, D.A., Gornbein, J., 1994. The Neuropsychiatric Inventory: comprehensive assessment of psychopathology in dementia. Neurology 44, 2308–2314.

Davis, M.H., 1983. Measuring individual differences in empathy: evidence for a multidimensional approach. J. Pers. Soc. Psychol. 44:113–126. http://dx.doi.org/10.1037/0022-3514.44.1.113.

Dean, D.C., Jerskey, B.A., Chen, K., Protas, H., Thiyyagura, P., Roontiva, A., O'Muircheartaigh, J., Dirks, H., Waskiewicz, N., Lehman, K., Siniard, A.L., Turk, M.N., Hua, X., Madsen, S.K., Thompson, P.M., Fleisher, A.S., Huentelman, M.J., Deoni, S.C.L., Reiman, E.M., 2014. Brain differences in infants at differential genetic risk for late-onset Alzheimer disease: a cross-sectional imaging study. JAMA Neurol. 71:11–22. http://dx.doi.org/10.1001/jamaneurol.2013.4544.

DeJesus-Hernandez, M., Mackenzie, I.R., Boeve, B.F., Boxer, A.L., Baker, M., Rutherford, N.J., Nicholson, A.M., Finch, N.A., Flynn, H., Adamson, J., Kouri, N., Wojtas, A., Sengdy, P., Hsiung, G.-Y.R., Karydas, A., Seeley, W.W., Josephs, K.A., Coppola, G., Geschwind, D.H., Wszolek, Z.K., Feldman, H., Knopman, D.S., Petersen, R.C., Miller, B.L., Dickson, D.W., Boylan, K.B., Graff-Radford, N.R., Rademakers, R., 2011. Expanded GGGGCC hexanucleotide repeat in noncoding region of C9ORF72 causes chromosome 9p-linked FTD and ALS. Neuron:1–12 http://dx.doi.org/10.1016/j.neuron.2011.09.011.

Dopper, E.G.P., Rombouts, S.A.R.B., Jiskoot, L.C., den Heijer, T., de Graaf, J.R.A., de Koning, I., Hammerschlag, A.R., Seelaar, H., Seeley, W.W., Veer, I.M., van Buchem, M.A., Rizzu, P., van Swieten, J.C., 2014. Structural and functional brain connectivity in presymptomatic familial frontotemporal dementia. Neurology 83:e19–e26. http://dx.doi.org/10.1212/WNL.0000000000000583.

Farb, N.A.S., Grady, C.L., Strother, S., Tang-Wai, D.F., Masellis, M., Black, S., Freedman, M., Pollock, B.G., Campbell, K.L., Hasher, L., Chow, T.W., 2013. Abnormal network connectivity in frontotemporal dementia: evidence for prefrontal isolation. Cortex 49: 1856–1873. http://dx.doi.org/10.1016/j.cortex.2012.09.008.

Folstein, M.F., Robins, L.N., Helzer, J.E., 1983. The Mini-Mental State Examination. Arch. Gen. Psychiatry 40, 812.

Gupta, C.N., Calhoun, V.D., Rachakonda, S., Chen, J., Patel, V., Liu, J., Segall, J., Franke, B., Zwiers, M.P., Arias-Vasquez, A., Buitelaar, J., Fisher, S.E., Fernandez, G., van Erp, T.G.M., Potkin, S., Ford, J., Mathalon, D., McEwen, S., Lee, H.J., Mueller, B.A., Greve, D.N., Andreassen, O., Agartz, I., Gollub, R.L., Sponheim, S.R., Ehrlich, S., Wang, L., Pearlson, G., Glahn, D.C., Sprooten, E., Mayer, A.R., Stephen, J., Jung, R.E., Canive, J., Bustillo, J., Turner, J.A., 2014. Patterns of Gray Matter Abnormalities in Schizophrenia Based on an International Mega-analysis. Schizophr. Bull. http://dx.doi.org/10.1093/schbul/sbu177.

Habas, C., Kamdar, N., Nguyen, D., Prater, K., Beckmann, C.F., Menon, V., Greicius, M.D., 2009. Distinct cerebellar contributions to intrinsic connectivity networks. J. Neurosci. 29:8586–8594. http://dx.doi.org/10.1523/JNEUROSCI.1868-09.2009.

Hensman Moss, D.J., Poulter, M., Beck, J., Hehir, J., Polke, J.M., Campbell, T., Adamson, G., Mudanohwo, E., McColgan, P., Haworth, A., Wild, E.J., Sweeney, M.G., Houlden, H., Mead, S., Tabrizi, S.J., 2014. C9orf72 expansions are the most common genetic cause of Huntington disease phenocopies. Neurology 82:292–299. http://dx.doi.org/10.1212/WNL.0000000000000061.

Irwin, D.J., McMillan, C.T., Brettschneider, J., Libon, D.J., Powers, J., Rascovsky, K., Toledo, J.B., Boller, A., Bekisz, J., Chandrasekaran, K., Wood, E.M., Shaw, L.M., Woo, J.H., Cook, P.A., Wolk, D.A., Arnold, S.E., Van Deerlin, V.M., McCluskey, L.F., Elman, L., Lee, V.M.Y., Trojanowski, J.Q., Grossman, M., 2013. Cognitive decline and reduced survival in C9orf72 expansion frontotemporal degeneration and amyotrophic lateral sclerosis. J. Neurol. Neurosurg. Psychiatry 84:163–169. http://dx.doi.org/10.1136/jnnp-2012-303507.

Jack, C.R., Petersen, R.C., Xu, Y.C., Waring, S.C., O'Brien, P.C., Tangalos, E.G., Smith, G.E., Ivnik, R.J., Kokmen, E., 1997. Medial temporal atrophy on MRI in normal aging and very mild Alzheimer's disease. Neurology 49, 786–794.

Kessler, R.C., McGonagle, K.A., Zhao, S., Nelson, C.B., Hughes, M., Eshleman, S., Wittchen, H.U., Kendler, K.S., 1994. Lifetime and 12-month prevalence of DSM-III-R psychiatric disorders in the United States. Results from the National Comorbidity Survey. Arch. Gen. Psychiatry 51, 8–19.

Knopman, D.S., Kramer, J.H., Boeve, B.F., Caselli, R.J., Graff-Radford, N.R., Mendez, M.F., Miller, B.L., Mercaldo, N., 2008. Development of methodology for conducting clinical trials in frontotemporal lobar degeneration. Brain 131:2957–2968. http://dx.doi.org/10.1093/brain/awn234.

Lee, S.E., Khazenzon, A.M., Trujillo, A.J., Guo, C.C., Yokoyama, J.S., Sha, S.J., Takada, L.T., Karydas, A.M., Block, N.R., Coppola, G., Pribadi, M., Geschwind, D.H., Rademakers, R., Fong, J.C., Weiner, M.W., Boxer, A.L., Kramer, J.H., Rosen, H.J., Miller, B.L., Seeley, W.W., 2014. Altered network connectivity in frontotemporal dementia with C9orf72 hexanucleotide repeat expansion. Brain 137:3047–3060. http://dx.doi.org/10.1093/brain/awu248.

Mahoney, C.J., Beck, J., Rohrer, J.D., Lashley, T., Mok, K., Shakespeare, T., Yeatman, T., Warrington, E.K., Schott, J.M., Fox, N.C., Rossor, M.N., Hardy, J., Collinge, J., Revesz, T., Mead, S., Warren, J.D., 2012. Frontotemporal dementia with the C9ORF72 hexanucleotide repeat expansion: clinical, neuroanatomical and neuropathological features. Brain 135:736–750. http://dx.doi.org/10.1093/brain/awr361.

Mahoney, C.J., Simpson, I.J.A., Nicholas, J.M., Fletcher, P.D., Downey, L.E., Golden, H.L., Clark, C.N., Schmitz, N., Rohrer, J.D., Schott, J.M., Zhang, H., Ourselin, S., Warren, J.D., Fox, N.C., 2014. Longitudinal diffusion tensor imaging in frontotemporal dementia. Ann. Neurol. 77:33–46. http://dx.doi.org/10.1002/ana.24296.

Maior, R.S., Hori, E., Tomaz, C., Ono, T., Nishijo, H., 2010. Behavioural brain research. Behav. Brain Res. 215:129–135. http://dx.doi.org/10.1016/j.bbr.2010.07.009.

Majounie, E., Renton, A.E., Mok, K., Dopper, E.G., Waite, A., Rollinson, S., Chiò, A., Restagno, G., Nicolaou, N., Simón-Sánchez, J., van Swieten, J.C., Abramzon, Y., Johnson, J.O., Sendtner, M., Pamphlett, R., Orrell, R.W., Mead, S., Sidle, K.C., Houlden, H., Rohrer, J.D., Morrison, K.E., Pall, H., Talbot, K., Ansorge, O., The Chromosome 9-ALS/FTD Consortium, The French research network on FTLD/FTLD/ALS, the ITALSGEN consortium, Hernandez, D.G., Arepalli, S., Sabatelli, M., Mora, G., Corbo, M., Giannini, F., Calvo, A., Englund, E., Borghero, G., Floris, G.L., Remes, A.M., Laaksovirta, H., McCluskey, L., Trojanowski, J.Q., Van Deerlin, V.M., Schellenberg, G.D., Nalls, M.A., Drory, V.E., Lu, C.-S., Yeh, T.-H., Ishiura, H., Takahashi, Y., Tsuji, S., Le Ber, I., Brice, A., Drepper, C., Williams, N., Kirby, J., Shaw, P., Hardy, J., Tienari, P.J., Heutink, P., Morris, H.R., Pickering-Brown, S., Traynor, B.J., 2012. Frequency of the C9orf72 hexanucleotide repeat expansion in patients with amyotrophic lateral sclerosis and frontotemporal dementia: a cross-sectional study. Lancet Neurol. 11:323–330. http://dx.doi.org/10.1016/S1474-4422(12)70043-1.

Miller, J.A., Ding, S.-L., Sunkin, S.M., Smith, K.A., Ng, L., Szafer, A., Ebbert, A., Riley, Z.L., Royall, J.J., Aiona, K., Arnold, J.M., Bennet, C., Bertagnolli, D., Brouner, K., Butler, S., Caldejon, S., Carey, A., Cuhaciyan, C., Dalley, R.A., Dee, N., Dolbeare, T.A., Facer, B.A.C., Feng, D., Fliss, T.P., Gee, G., Goldy, J., Gourley, L., Gregor, B.W., Gu, G., Howard, R.E., Jochim, J.M., Kuan, C.L., Lau, C., Lee, C.-K., Lee, F., Lemon, T.A., Lesnar, P., McMurray, B., Mastan, N., Mosqueda, N., Naluai-Cecchini, T., Ngo, N.-K., Nyhus, J., Oldre, A., Olson, E., Parente, J., Parker, P.D., Parry, S.E., Stevens, A., Pletikos, M., Reding, M., Roll, K., Sandman, D., Sarreal, M., Shapouri, S., Shapovalova, N.V., Shen, E.H., Sjoquist, N., Slaughterbeck, C.R., Smith, M., Sodt, A.J., Williams, D., Zöllei, L., Fischl, B., Gerstein, M.B., Geschwind, D.H., Glass, I.A., Hawrylycz, M.J., Hevner, R.F., Huang, H., Jones, A.R., Knowles, J.A., Levitt, P., Phillips, J.W., Sestan, N., Wohnoutka, P., Dang, C., Bernard, A., Hohmann, J.G., Lein, E.S., 2014. Transcriptional landscape of the prenatal human brain. Nature 508:199–206. http://dx.doi.org/10.1038/nature13185.

Mufson, E.J., Mesulam, M.M., 1984. Thalamic connections of the insula in the rhesus monkey and comments on the paralimbic connectivity of the medial pulvinar nucleus. J. Comp. Neurol. 227:109–120. http://dx.doi.org/10.1002/cne.902270112.

O'Rourke, J.G., Bogdanik, L., Yáñez, A., Lall, D., Wolf, A.J., Muhammad, A.K.M.G., Ho, R., Carmona, S., Vit, J.P., Zarrow, J., Kim, K.J., Bell, S., Harms, M.B., Miller, T.M., Dangler, C.A., Underhill, D.M., Goodridge, H.S., Lutz, C.M., Baloh, R.H., 2016. C9orf72 is required for proper macrophage and microglial function in mice. Science 351:1324–1329. http://dx.doi.org/10.1126/science.aaf1064.

Pierpaoli, C., Basser, P.J., 1996. Toward a quantitative assessment of diffusion anisotropy. Magn. Reson. Med. 36, 893–906.

Poline, J.B., Worsley, K.J., Evans, A.C., Friston, K.J., 1997. Combining spatial extent and peak intensity to test for activations in functional imaging. NeuroImage 5:83–96. http://dx.doi.org/10.1006/nimg.1996.0248.

Proudfoot, M., Gutowski, N.J., Edbauer, D., Hilton, D.A., Stephens, M., Rankin, J., Mackenzie, I.R.A., 2014. Early dipeptide repeat pathology in a frontotemporal dementia kindred with C9ORF72 mutation and intellectual disability. Acta Neuropathol. 127:451–458. http://dx.doi.org/10.1007/s00401-014-1245-7.

Renton, A.E., Majounie, E., Waite, A., Simón-Sánchez, J., Rollinson, S., Gibbs, J.R., Schymick, J.C., Laaksovirta, H., van Swieten, J.C., Myllykangas, L., Kalimo, H., Paetau, A., Abramzon, Y., Remes, A.M., Kaganovich, A., Scholz, S.W., Duckworth, J., Ding, J., Harmer, D.W., Hernandez, D.G., Johnson, J.O., Mok, K., Ryten, M., Trabzuni, D., Guerreiro, R.J., Orrell, R.W., Neal, J., Murray, A., Pearson, J., Jansen, I.E., Sondervan, D., Seelaar, H., Blake, D., Young, K., Halliwell, N., Callister, J.B., Toulson, G., Richardson, A., Gerhard, A., Snowden, J., Mann, D., Neary, D., Nalls, M.A., Peuralinna, T., Jansson, L., Isoviita, V.-M., Kaivorinne, A.-L., Hölttä-Vuori, M., Ikonen, E., Sulkava, R., Benatar, M., Wuu, J., Chiò, A., Restagno, G., Borghero, G., Sabatelli, M., Heckerman, D., Rogaeva, E., Zinman, L., Rothstein, J.D., Sendtner, M., Drepper, C., Eichler, E.E., Alkan, C., Abdullaev, Z., Pack, S.D., Dutra, A., Pak, E., Hardy, J., Singleton, A., Williams, N.M., Heutink, P., Pickering-Brown, S., Morris, H.R., Tienari, P.J., Traynor, B.J., Consortium28, T.I, 2011. A hexanucleotide repeat expansion in C9ORF72 is the cause of chromosome 9p21-Linked ALS-FTD. Neuron:1–12 http://dx.doi.org/10.1016/j.neuron.2011.09.010.

Rohrer, J.D., Nicholas, J.M., Cash, D.M., van Swieten, J., Dopper, E., Jiskoot, L., van Minkelen, R., Rombouts, S.A., Cardoso, M.J., Clegg, S., Espak, M., Mead, S., Thomas, D.L., De Vita, E., Masellis, M., Black, S.E., Freedman, M., Keren, R., MacIntosh, B.J., Rogaeva, E., Tang-Wai, D., Tartaglia, M.C., Laforce, R., Tagliavini, F., Tiraboschi, P., Redaelli, V., Prioni, S., Grisoli, M., Borroni, B., Padovani, A., Galimberti, D., Scarpini, E., Arighi, A., Fumagalli, G., Rowe, J.B., Coyle-Gilchrist, I., Graff, C., Fallström, M., Jelic, V., Ståhlbom, A.K., Andersson, C., Thonberg, H., Lilius, L., Frisoni, G.B., Pievani, M., Bocchetta, M., Benussi, L., Ghidoni, R., Finger, E., Sorbi, S., Nacmias, B., Lombardi, G., Polito, C., Warren, J.D., Ourselin, S., Fox, N.C., Rossor, M.N., 2015. Presymptomatic cognitive and neuroanatomical changes in genetic frontotemporal dementia in the genetic Frontotemporal dementia initiative (GENFI) study: a cross-sectional analysis. Lancet Neurol. 14:253–262. http://dx.doi.org/10.1016/S1474-4422(14)70324-2.

Romanski, L.M., Giguere, M., Bates, J.F., Goldman-Rakic, P.S., 1997. Topographic organization of medial pulvinar connections with the prefrontal cortex in the rhesus monkey. J. Comp. Neurol. 379, 313–332.

Seeley, W.W., Crawford, R., Rascovsky, K., Kramer, J.H., Weiner, M., Miller, B.L., Gorno-Tempini, M.L., 2008. Frontal paralimbic network atrophy in very mild behavioral variant frontotemporal dementia. Arch. Neurol. 65:249–255. http://dx.doi.org/10.1001/archneurol.2007.38.

Seeley, W.W., Crawford, R.K., Zhou, J., Miller, B.L., Greicius, M.D., 2009. Neurodegenerative diseases target large-scale human brain networks. Neuron 62:42–52. http://dx.doi.org/10.1016/j.neuron.2009.03.024.

Seeley, W.W., Menon, V., Schatzberg, A.F., Keller, J., Glover, G.H., Kenna, H., Reiss, A.L., Greicius, M.D., 2007. Dissociable intrinsic connectivity networks for salience processing and executive control. J. Neurosci. 27:2349–2356. http://dx.doi.org/10.1523/JNEUROSCI.5587-06.2007.

Sha, S.J., Takada, L.T., Rankin, K.P., Yokoyama, J.S., Rutherford, N.J., Fong, J.C., Khan, B., Karydas, A., Baker, M.C., DeJesus-Hernandez, M., Pribadi, M., Coppola, G., Geschwind, D.H., Rademakers, R., Lee, S.E., Seeley, W., Miller, B.L., Boxer, A.L., 2012. Frontotemporal dementia due to C9ORF72 mutations: clinical and imaging features. Neurology 79:1002–1011. http://dx.doi.org/10.1212/WNL.0b013e318268452e.

Simón-Sánchez, J., Dopper, E.G.P., Cohn-Hokke, P.E., Hukema, R.K., Nicolaou, N., Seelaar, H., de Graaf, J.R.A., de Koning, I., van Schoor, N.M., Deeg, D.J.H., Smits, M., Raaphorst, J., van den Berg, L.H., Schelhaas, H.J., De Die-Smulders, C.E.M., Majoor-Krakauer, D., Rozemuller, A.J.M., Willemsen, R., Pijnenburg, Y.A.L., Heutink, P., van Swieten, J.C., 2012. The clinical and pathological phenotype of C9ORF72 hexanucleotide repeat expansions. Brain 135:723–735. http://dx.doi.org/10.1093/brain/awr353.

Smith, S.M., Jenkinson, M., Johansen-Berg, H., Rueckert, D., Nichols, T.E., Mackay, C.E., Watkins, K.E., Ciccarelli, O., Cader, M.Z., Matthews, P.M., Behrens, T.E.J., 2006. Tract-based spatial statistics: voxelwise analysis of multi-subject diffusion data. NeuroImage 31:1487–1505. http://dx.doi.org/10.1016/j.neuroimage.2006.02.024.

Snowden, J.S., Rollinson, S., Thompson, J.C., Harris, J.M., Stopford, C.L., Richardson, A.M.T., Jones, M., Gerhard, A., Davidson, Y.S., Robinson, A., Gibbons, L., Hu, Q., Duplessis, D., Neary, D., Mann, D.M.A., Pickering-Brown, S.M., 2012. Distinct clinical and pathological characteristics of frontotemporal dementia associated with C9ORF72 mutations. Brain 135:693–708. http://dx.doi.org/10.1093/brain/awr355.

Van Dijk, K.R.A., Sabuncu, M.R., Buckner, R.L., 2012. The influence of head motion on intrinsic functional connectivity MRI. NeuroImage 59:431–438. http://dx.doi.org/10.1016/j.neuroimage.2011.07.044.

Van Le, Q., Isbell, L.A., Matsumoto, J., Nguyen, M., Hori, E., Maior, R.S., Tomaz, C., Tran, A.H., Ono, T., Nishijo, H., 2013. Pulvinar neurons reveal neurobiological evidence of past selection for rapid detection of snakes. Proc. Natl. Acad. Sci. U. S. A. 110:19000–19005. http://dx.doi.org/10.1073/pnas.1312648110.

Vatsavayai, S.C., Yoon, S.J., Gardner, R.C., Gendron, T.F., JN, V., Trujillo, A.J., Pribadi, M., Phillips, J.J., Gaus, S.E., Hixson, J.D., Garcia, P.A., Rabinovici, G.D., Rabinovici, Coppola, G., Geschwind, D.H., Petrucelli, L., Miller, B.L., Seeley, W.W., 2016. Timing and significance of pathological features in C9ORF72 expansion-associated frontotemporal dementia. Brain:3202–3216 http://dx.doi.org/10.1093/brain/aww250.

Walhout, R., Schmidt, R., Westeneng, H.-J., Verstraete, E., Seelen, M., van Rheenen, W., de Reus, M.A., van Es, M.A., Hendrikse, J., Veldink, J.H., van den Heuvel, M.P., van den Berg, L.H., 2015. Brain morphologic changes in asymptomatic C9orf72 repeat expansion carriers. Neurology:1–9 http://dx.doi.org/10.1212/WNL.0000000000002135.

Whitwell, J.L., Josephs, K.A., Avula, R., Tosakulwong, N., Weigand, S.D., Senjem, M.L., Vemuri, P., Jones, D.T., Gunter, J.L., Baker, M., Wszolek, Z.K., Knopman, D.S., Rademakers, R., Petersen, R.C., Boeve, B.F., Jack, C.R., 2011. Altered functional connectivity in asymptomatic MAPT subjects: a comparison to bvFTD. Neurology 77:866–874. http://dx.doi.org/10.1212/WNL.0b013e31822c61f2.

Whitwell, J.L., Weigand, S.D., Boeve, B.F., Senjem, M.L., Gunter, J.L., DeJesus-Hernandez, M., Rutherford, N.J., Baker, M., Knopman, D.S., Wszolek, Z.K., Parisi, J.E., Dickson, D.W., Petersen, R.C., Rademakers, R., Jack, C.R., Josephs, K.A., 2012. Neuroimaging signatures of frontotemporal dementia genetics: C9ORF72, tau, progranulin and sporadics. Brain 135:794–806. http://dx.doi.org/10.1093/brain/aws001.

Zhou, J., Greicius, M.D., Gennatas, E.D., Growdon, M.E., Jang, J.Y., Rabinovici, G.D., Kramer, J.H., Weiner, M., Miller, B.L., Seeley, W.W., 2010. Divergent network connectivity changes in behavioural variant frontotemporal dementia and Alzheimer's disease. Brain 133:1352–1367. http://dx.doi.org/10.1093/brain/awq075.

Zielinski, B.A., Gennatas, E.D., Zhou, J., Seeley, W.W., 2010. Network-level structural covariance in the developing brain. Proc. Natl. Acad. Sci. U. S. A. 107:18191–18196. http://dx.doi.org/10.1073/pnas.1003109107.